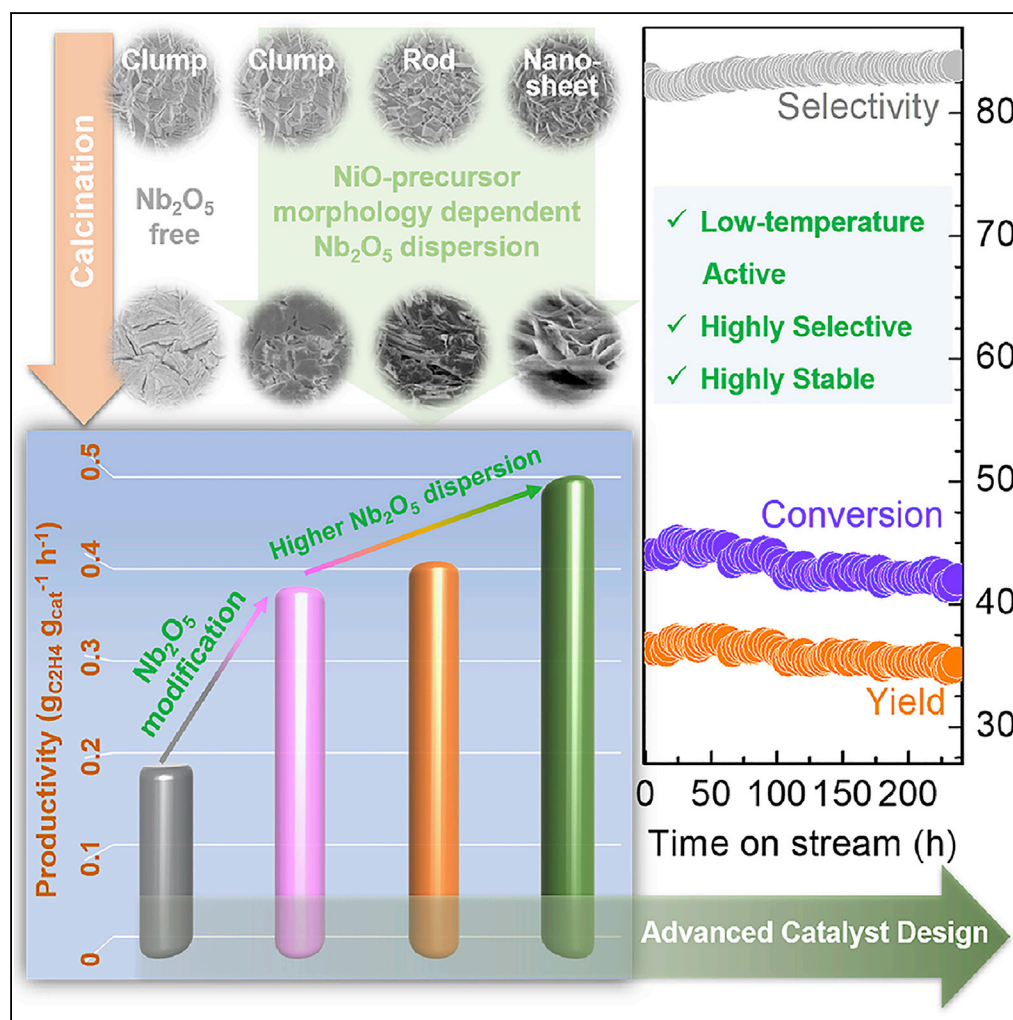


Article

Oxidative Dehydrogenation of Ethane: Superior Nb₂O₅-NiO/Ni-Foam Catalyst Tailored by Tuning Morphology of NiO-Precursors Grown on a Ni-Foam



Zhiqiang Zhang,
Guofeng Zhao,
Weidong Sun, Ye
Liu, Yong Lu

gfzhao@chem.ecnu.edu.cn
(G.Z.)
ylu@chem.ecnu.edu.cn (Y.L.)

HIGHLIGHTS

A series of Nb₂O₅-NiO/
Ni-foam catalysts are
developed for the ODE
reaction

Catalysts are obtained by
Nb₂O₅ modification of
NiO-precursors grown
onto Ni-foam

Thinning NiO-precursors
dramatically improves the
ethylene selectivity

Non-selective O₂⁻ species
are markedly reduced with
enhanced Nb₂O₅-NiO
interaction

Article

Oxidative Dehydrogenation of Ethane: Superior Nb₂O₅-NiO/Ni-Foam Catalyst Tailored by Tuning Morphology of NiO-Precursors Grown on a Ni-Foam

Zhiqiang Zhang,¹ Guofeng Zhao,^{2,*} Weidong Sun,¹ Ye Liu,¹ and Yong Lu^{1,2,3,*}

SUMMARY

Large-scale shale gas exploitation greatly enriches ethane resources, making the oxidative dehydrogenation of ethane to ethylene quite fascinating, but the qualified catalyst with unique combination of enhanced activity/selectivity, enhanced heat transfer, and low pressure drop presents a grand challenge. Herein, a high-performance Nb₂O₅-NiO/Ni-foam catalyst engineered from nano- to macroscale for this reaction is tailored by finely tuning the performance-relevant Nb₂O₅-NiO interaction that is strongly dependent on NiO-precursor morphology. Three NiO-precursors of different morphologies (clump, rod, and nanosheet) were directly grown onto Ni-foam followed by Nb₂O₅ modification to obtain the catalyst products. Notably, the one from the NiO-precursor of nanosheet achieves the highest ethylene yield, in nature, because of markedly diminished unselective oxygen species due to enhanced interaction between Nb₂O₅ and NiO nanosheet. An advanced catalyst is developed by further thinning the NiO-precursor nanosheet, which achieves 60% conversion with 80% selectivity and is stable for at least 240 h.

INTRODUCTION

Ethylene (C₂H₄) is regarded as the most important petrochemical platform molecule to produce diverse commodity chemicals such as polyethylene, ethylene oxide, vinyl chloride, and polystyrene, with global demand of 153 million tons in 2016 and net added demand of about 5.2 million tons every year (Xu, 2017). Nowadays, its universal production in industry is based on the steam cracking of oil-based naphtha. However, the oil resource is increasingly dwindling, and thus it has turned out to be a hotspot in modern industries to pave the way for efficient and ecofriendly utilization of the nonoil resources (e.g., natural gas, coal, and renewable biomass) to produce ethylene with the aid of effective catalytic processes. Ethane (C₂H₆) is abundant in natural gas, and in particular, the shale gas revolution in recent years greatly enriches ethane resources (Sattler et al., 2014). Therefore, ethane-to-ethylene conversion (in terms of oxidative dehydrogenation of ethane [ODE], catalytic dehydrogenation, and steam cracking) tantalizes global enthusiasm. The latter two suffer from their thermodynamic constraints and high operation temperature (>700°C), and the ODE is thus more competitive, benefitting from its oxidative feature that can cast off the thermodynamic limitation and allow lower operation temperature (350°C–550°C) (Heynderickx et al., 2005).

However, controlling the ethylene selectivity for ODE reaction represents the grandest challenge because the excessive oxidation of ethylene to carbon dioxide is thermodynamically and kinetically favorable. Therefore, developing a qualified catalyst with high activity and selectivity is the goal of most efforts for this reaction. To date, various catalysts have been explored (such as alkaline-/rare-earth metal oxides, Mulla et al., 2001, Gaab et al., 2003; noble metals, Fu et al., 2013; and transition metal oxides, Liu et al., 2003; Nakamura et al., 2006), and NiO-based catalysts are the most attractive owing to its low operation temperature, simple preparation, and low cost (Heracleous and Lemonidou, 2006, 2010; Savova et al., 2010; Zhu et al., 2012). However, NiO alone mainly yields carbon dioxide due to the large amount of electrophilic (unselective) oxygen species (Heracleous and Lemonidou, 2006, 2010; Savova et al., 2010; Zhu et al., 2012). Many kinds of oxides were doped into NiO to tune the oxidative properties of oxygen species. Lemonidou et al. explored a series of alter-valent cations such as Li, Mg, Al, Ga, Ti, Ta, and Nb (Heracleous and Lemonidou, 2010), and the unselective oxygen amount on NiO surface declines along with the increase in dopant cations' valence. Accordingly, the Nb₂O₅-doped catalyst offers the highest ODE performance such as 78% ethylene selectivity and 33% ethane conversion at 350°C (Savova et al., 2010). They further proposed that Nb doping into NiO lattice by filling the cationic vacancies on

¹Shanghai Key Laboratory of Green Chemistry and Chemical Processes, School of Chemistry and Molecular Engineering, East China Normal University, Shanghai 200062, China

²School of Chemistry and Molecular Engineering, East China Normal University, Shanghai 200062, China

³Lead Contact

*Correspondence: gzhao@chem.ecnu.edu.cn (G.Z.), ylu@chem.ecnu.edu.cn (Y.L.)
<https://doi.org/10.1016/j.isci.2019.09.021>



defective non-stoichiometric NiO surface and/or substituting Ni atoms reduces the amount of unselective oxygen (Zhu et al., 2012; Heracleous and Lemonidou, 2006). However, such Nb₂O₅-NiO catalysts suffer from poor stability due to their sintering deactivation (Heracleous and Lemonidou, 2006, 2010; Savova et al., 2010; Zhu et al., 2012).

Despite the above-mentioned interesting advances, the real-world use of these catalysts still remains a challenge as their poor thermal conductivity is detrimental to rapid dissipation of reaction heat released in this strongly exothermic ODE reaction ($\Delta H = -104 \text{ kJ mol}^{-1}$), which causes severe hotspots in the catalyst bed and therefore leads to the ethylene excessive oxidation while releasing more heat. Recently, the development of structured catalyst based on the monolithic metal-foam has been attracting great interest in heterogeneous catalysis because of the intensified heat transfer, which is favorable to tailor catalysts for strongly exothermic reactions (Chen et al., 2019; Zhao et al., 2016; Zhang et al., 2018a, 2018b). However, the main issue is how to make these promising metal-foam qualified catalysts, or more concretely, how to fabricate the highly active and selective NiO-based nanocomposites onto foam surface.

Herein, we demonstrate the remarkable improvement of the Nb₂O₅-NiO/Ni-foam catalyst performance for ODE reaction, by finely tuning the Nb₂O₅-NiO interaction by morphology-controllable growth of NiO-precursors onto Ni-foam.

RESULTS

Synthesis, Morphology, and Structural Features of the Ni-Foam Structured NiO-Precursor and Catalysts

First, three kinds of NiO-precursors with different morphologies (i.e., clump for Ni(OH)₂, rod for NiC₂O₄, nanosheet for nickel terephthalate (Ni-Tp), identified by X-ray diffraction [XRD] in Figure S1) were controllably and endogenously grown onto a Ni-foam (100 pores per inch). Against the smooth surface of Ni-foam (Figures 1A–1C), clearly, the *in situ* growth of three morphology-different NiO-precursor layers on the foam struts succeeds clump with dense stacking for Ni(OH)₂ layer by ammonia evaporation method (Figures 1D, 1G, and 1J), rod with diameter of about 450 nm for NiC₂O₄ layer by hydrothermal method (Figures 1E, 1H, and 1K), and nanosheet of thickness 30 nm for Ni-Tp layer by solvothermal method (Figures 1F, 1I, and 1L). Moreover, unlike the dense layer feature of the Ni(OH)₂ clump and NiC₂O₄ rod, the Ni-Tp nanosheets stand upright and irregularly cross-link each other to form honeycomb-like porous layer. Not surprisingly, the Ni-Tp/Ni-foam delivers a specific surface area (SSA) of 6.3 m² g⁻¹ much higher than 1–2 m² g⁻¹ for the Ni(OH)₂/Ni-foam and NiC₂O₄/Ni-foam (Table 1).

Subsequently, niobium ammonium oxalate was wet-impregnated onto the above-obtained Ni(OH)₂/Ni-foam, NiC₂O₄/Ni-foam, and Ni-Tp/Ni-foam at a Nb₂O₅ content of 5 wt. % (including the Ni-foam mass), followed by drying overnight and calcining in air at 450°C, to form Ni-foam-structured Nb₂O₅-NiO catalysts (Figures 1M–1U). These catalysts are denoted as Nb₂O₅-NiO/Ni-foam-C (clump), Nb₂O₅-NiO/Ni-foam-R (rod), and Nb₂O₅-NiO/Ni-foam-NS (nanosheet), which all possess equivalent NiO content (~21 wt. %, including Ni-foam mass; Table 1). The NiO and Ni (from Ni-foam) phases are clearly detected by XRD for all three catalysts, whereas no Nb₂O₅ diffraction peaks are observed, indicating its high dispersion or amorphous structure (Figure S2) (Liu et al., 2016). Notably, the Ni(OH)₂-, NiC₂O₄-, and Ni-Tp-derived nano-NiO aggregations show well-preserved clump-, rod- and nanosheet-morphologies regardless of Nb₂O₅ introduction (Figures 1M–1O). In addition, the Nb₂O₅-NiO ensembles show porous feature in association with the thermolysis of their precursors (Figures 1P–1R) thereby leading to a visible increase in their SSA (Table 1).

Interestingly, the Nb₂O₅-NiO/Ni-foam-NS achieves an SSA of 20.8 m² g⁻¹, much higher than 12–13 m² g⁻¹ seen with the other two catalysts (Table 1). The enhanced surface area can be related to the fact that the nanosheet-like morphology of Ni-Tp/Ni-foam not only favors the formation of catalyst with high SSA (see NiO/Ni-foam-NS, Table 1) but also is helpful for highly dispersing Nb₂O₅-precursor onto the Ni-Tp nanosheet to hinder the crystallization of NiO during the calcination process (Solsona et al., 2011, 2012) (Table 1). Not surprisingly, the Nb₂O₅-NiO/Ni-foam-NS catalyst provides an average NiO size of 13.5 nm, smaller than that of ~20 nm for the Nb₂O₅-NiO/Ni-foam-C and Nb₂O₅-NiO/Ni-foam-R (Table 1). Nevertheless, the NiO/Ni-foam-NS obtained by calcining the Ni-Tp/Ni-foam in air at 450°C offers an average NiO size of ~20 nm, being compatible to that seen with the ones derived from

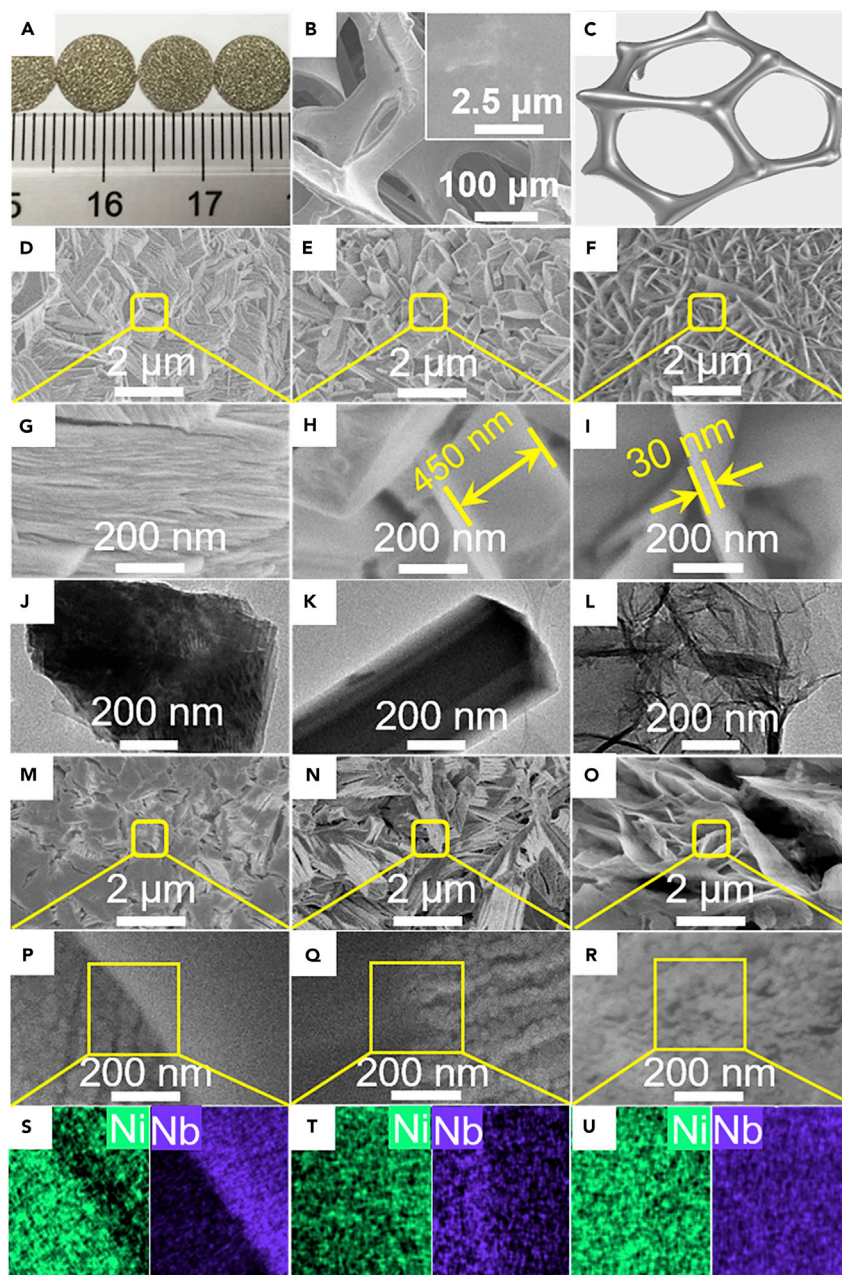


Figure 1. The Structure and Morphological Features of Various NiO-Precursors and Nb₂O₅-NiO/Ni-Foam Catalysts

(A–C) (A) Optical photograph, (B) scanning electron microscopic (SEM) image, and (C) schematic illustration of network of the pristine Ni-foam.

(D, G, and J) (D and G) SEM and (J) transmission electron microscopic (TEM) images of Ni(OH)₂/Ni-foam.

(E, H, and K) (E and H) SEM and (K) TEM images of NiC₂O₄/Ni-foam.

(F, I, and L) (F and I) SEM and (L) TEM images of Ni-Tp/Ni-foam.

(M, P, and S) (M and P) SEM and (S) energy-dispersive X-ray (EDX) images of Nb₂O₅-NiO/Ni-foam-C.

(N, Q, and T) (N and Q) SEM and (T) EDX images of Nb₂O₅-NiO/Ni-foam-R.

(O, R, and U) (O and R) SEM and (U) EDX images of Nb₂O₅-NiO/Ni-foam-NS.

Catalyst	NiO Loading (wt. %) ^a	NiO Average Size (nm) ^b	Specific Surface Area (m ² g ⁻¹) ^c	NiO Lattice Constant (Å)	TOF ^d
Ni(OH) ₂ /Ni-foam	–	–	1.5	–	–
NiC ₂ O ₄ /Ni-foam	–	–	2.1	–	–
Ni-Tp/Ni-foam	–	–	6.3	–	–
NiO/Ni-foam-C	21.4	19.6	8.7	4.1767	0.61
NiO/Ni-foam-R	21.5	20.3	9.3	4.1768	0.64
NiO/Ni-foam-NS	21.1	19.5	10.7	4.1766	0.62
NiO/Ni-foam-F	20.6	20.9	10.1	4.1769	–
Nb ₂ O ₅ -NiO/Ni-foam-C	21.2	19.3	12.1	4.1753	0.91
Nb ₂ O ₅ -NiO/Ni-foam-R	20.9	20.4	13.3	4.1751	0.96
Nb ₂ O ₅ -NiO/Ni-foam-NS	20.8	13.5	20.8	4.1724	0.93
Nb ₂ O ₅ -NiO/Ni-foam-F	20.5	12.8	30.3	4.1721	0.94
Nb ₂ O ₅ -NiO/Ni-foam-F ^e	–	14.5	28.7	–	–

Table 1. Physicochemical Characteristics of the Ni-Foam Structured Catalysts

^aEstimated by H₂-TPR (Li et al., 2015) according to the reaction: H₂ + NiO = Ni + H₂O, given that Nb₂O₅ is normally considered to be an irreducible oxide (Zhang et al., 2018a, 2018b).

^bCalculated by Scherrer equation based on NiO (110) plane.

^cMeasured by N₂-BET method.

^dTOF (turnover frequency) is defined as the amount of ethylene formed per NiO site per hour (the detailed TOF calculations are provided in Supplemental Information and the related results are listed in Table S1); C₂H₆ conversion was controlled to be <5% at 300°C.

^eThe Nb₂O₅-NiO/Ni-foam-F after 240 h testing.

Ni(OH)₂/Ni-foam and NiC₂O₄/Ni-foam. This observation reveals that Nb₂O₅ introduction favors the decomposition of Ni-Tp nanosheets, rather than Ni(OH)₂-clump and NiC₂O₄-rod, to form smaller NiO nanoparticles. Moreover, the Nb₂O₅-NiO/Ni-foam-NS achieves more homogeneous NiO-Nb₂O₅ composites than the other two catalysts (Figures 1S–1U).

ODE Reaction Performance

The Nb₂O₅ modification dramatically improves the ethylene selectivity and slightly the ethane conversion while leading to a remarkable increase in the turnover frequency (TOF) for ethylene formation from ~0.62 h⁻¹ for the Nb₂O₅-free samples to 0.91–0.96 h⁻¹ at 300°C (Table 1 and Table S1; the detailed calculation method in the Supplemental Information). As shown in Figure 2, three Nb₂O₅-free samples all achieve almost identical ethane conversion and ethylene selectivity in the whole temperature range studied. In contrast, the Nb₂O₅-NiO/Ni-foam catalysts exhibit different ODE performance under identical reaction conditions, showing the NiO-precursor morphology dependence; the Nb₂O₅-NiO/Ni-foam-NS is obviously superior to the Nb₂O₅-NiO/Ni-foam-C and Nb₂O₅-NiO/Ni-foam-R catalysts (Figure 2), achieving a 58.4% ethane conversion and 75.4% ethylene selectivity at 425°C. In addition, compared with the very low productivity of only 0.18 g_{ethylene} g_{cat.}⁻¹ h⁻¹ over the Nb₂O₅-free NiO/Ni-foam catalysts, Nb₂O₅ modification gets the ethylene productivity doubled even more. The Nb₂O₅-NiO/Ni-foam-NS achieves the highest ethylene productivity of 0.46 g_{ethylene} g_{cat.}⁻¹ h⁻¹ (Figure S3).

Insight into the NiO-Precursor Morphology-Dependent Catalytic Performance

To reveal the underlying origin of the NiO-precursor morphology-dependent ODE catalysis on the above Nb₂O₅-NiO/Ni-foam catalysts, the amount and type of oxygen species were collaboratively probed by H₂-temperature-programmed reduction (H₂-TPR) and O₂-temperature-programmed desorption (O₂-TPD) (Zhu et al., 2012; Zhang et al., 2018a, 2018b). Clearly, whereas the Nb₂O₅-free NiO/Ni-foam samples show quite different NiO morphologies (Figure S4), they all possess identical reducibility (by H₂-TPR) and properties of surface oxygen species (by O₂-TPD), solidly evidenced by their almost same H₂-TPR

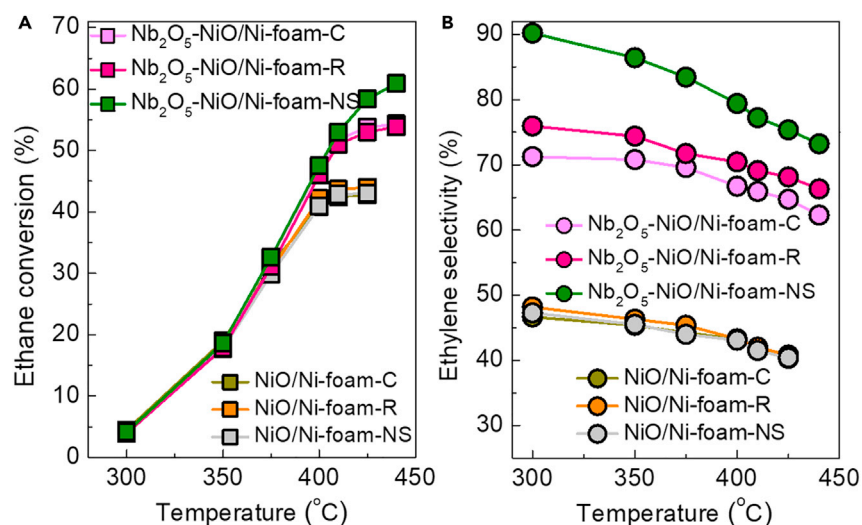


Figure 2. The ODE Performance of the Ni-Foam Structured Catalysts

(A and B) Temperature-dependent (A) ethane conversion and (B) ethylene selectivity. Reaction conditions: C₂H₆/O₂/N₂ of 1/1/8, GHSV of 9,000 cm³ g⁻¹ h⁻¹.

and O₂-TPD profiles (shape, peak area, and peak temperature; Figures 3A and 3B, profiles 1–3). It is thus not surprising that they achieve NiO-precursor morphology-independent ODE performance (Figure 2). In combining this information with the observation of NiO-precursor morphology dependences of distinct ODE performance after Nb₂O₅ modification, it is safe to say that the NiO-Nb₂O₅ interaction is sensitive to NiO-precursor morphology, which in nature is responsible for the distinct ODE performance for the Nb₂O₅-NiO/Ni-foam catalysts.

Indeed, the reducibility and properties of the surface oxygen species of the Nb₂O₅-NiO/Ni-foam catalysts show strong NiO-precursor morphology dependence (Figures 3A and 3B, profiles 4–6). The Nb₂O₅-NiO/Ni-foam-C offers a single H₂-TPR peak at 340°C with an 8°C delay compared with the NiO/Ni-foam, likely due to the weak Nb₂O₅-NiO interaction. The Nb₂O₅-NiO/Ni-foam-R delivers a main peak at 332°C and a weak shoulder at 358°C, suggesting the very limited local occurrence of moderate NiO-Nb₂O₅ interaction. In contrast, the Nb₂O₅-NiO/Ni-foam-NS provides a main peak at 371°C and a very weak one at only 297°C. It should be noted that the H₂ consumption is attributed exclusively to the NiO reduction because Nb₂O₅ reduction cannot occur under such conditions (Zhang et al., 2018a, 2018b). Particularly, the NiO size of the Nb₂O₅-NiO/Ni-foam-NS is 13.5 nm, smaller than 20 nm for the others. In general, the lattice oxygen of the smaller NiO nanocrystallites diffuses more efficiently than the larger ones (Zhu et al., 2012). So, the weak peak at 297°C is assignable to the small NiO species that interacted weakly with Nb₂O₅, whereas the main peak at 371°C is ascribable to the comprehensive occurrence of strong NiO-Nb₂O₅ interaction.

All catalysts with and without Nb₂O₅ modification deliver dual-peak O₂-TPD profiles, in which the peak at 342°C is assigned to O₂⁻ and the one at 543°C is assigned to O⁻ (Figure 3B) (Wu et al., 2012; Iwamoto et al., 1976). The O₂⁻ species have strong oxidizing electrophilicity and thus are considered to be non-selective oxygen species that favor the deep oxidation of product (Wu et al., 2012; Iwamoto et al., 1976). The amount and desorption behavior of O₂⁻ and O⁻ species are tuned markedly by Nb₂O₅ modification, showing clear NiO-precursor morphology dependence (Table S2 and Figure 3B). The desorbability of such two types of surface oxygen species is almost unchanged for the Nb₂O₅-NiO/Ni-foam-C and Nb₂O₅-NiO/Ni-foam-R, whereas their non-selective O₂⁻ amounts are markedly reduced in association with a slight decline of the O⁻ amount, when compared with the Nb₂O₅-free samples (Table S2 and Figure 3B). For Nb₂O₅-NiO/Ni-foam-NS, most notably, the Nb₂O₅ modification makes the non-selective O₂⁻ species almost disappear, but slightly decreases the selective O⁻ species, whereas lowers the desorption temperature of O⁻ species to 520°C by 23°C (Table S2 and Figure 3B). According to the Mars van Krevelen mechanism (Figure S5) (Zhu et al., 2012), the types of oxygen species determines the further reaction of ethyl radical to form ethylene (β-elimination) or CO₂ (C-C bond cleavage). It is not surprising that Nb₂O₅ modification and

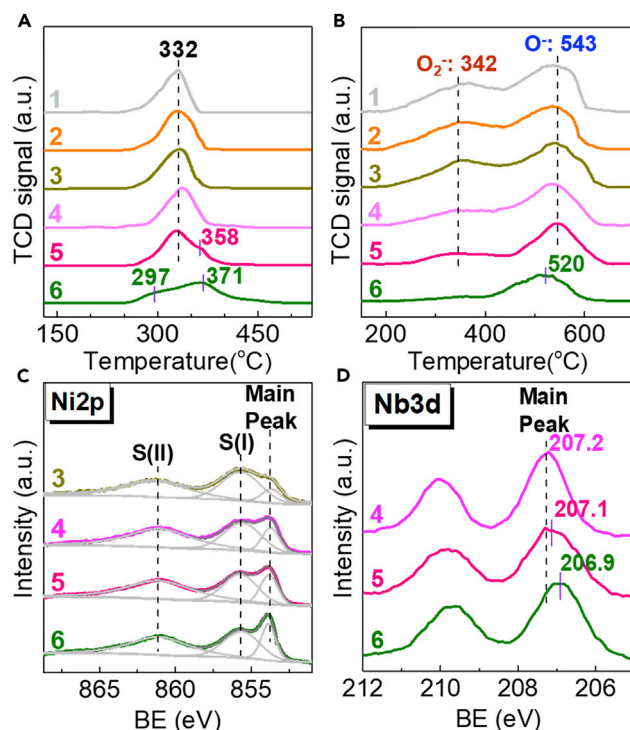


Figure 3. The Characterization Results of the Nb₂O₅-NiO/Ni-Foam Catalysts

(A–D) (A) H₂-TPR profiles, (B) O₂-TPD profiles, and XPS spectra of (C) Ni2p and (D) Nb3d of the catalysts of (1) NiO/Ni-foam-C, (2) NiO/Ni-foam-R, (3) NiO/Ni-foam-NS, (4) Nb₂O₅-NiO/Ni-foam-C, (5) Nb₂O₅-NiO/Ni-foam-R, and (6) Nb₂O₅-NiO/Ni-foam-NS.

thinning the NiO-precursor thickness are inclined to reduce the non-selective O₂⁻ species amount and form the ethylene via β-elimination.

In nature, tuning the NiO-precursor morphology from dense Ni(OH)₂ clump and NiC₂O₄ rod (450 nm) to Ni-Tp nanosheet (30 nm thickness) strengthens the NiO-Nb₂O₅ interaction thereby leading to almost elimination of the non-selective O₂⁻ species and meanwhile improving the mobility of the highly selective O⁻ species. Improved mobility of the O⁻ species (lowered desorption temperature, Figure 3B) (Wu et al., 2012; Skoufa et al., 2014) makes it more active than the other two catalysts, which in turn compensates the activity loss caused by the reduction of non-selective O₂⁻ and selective O⁻ species (Zhu et al., 2016). That is the reason why the Nb₂O₅-NiO/Ni-foam-NS catalyst always achieves higher conversion especially above 375°C (Figure 2A).

To further gain insight into the O₂⁻ reduction caused by Nb₂O₅-NiO interaction, the surfaces of the NiO/Ni-foam and Nb₂O₅-NiO/Ni-foam catalysts were probed by X-ray photoelectron spectroscopy (XPS). Figure 3C shows the Ni2p spectra of the catalyst samples. Three peaks are detected: main peak at binding energy (BE) of 853.8 eV for Ni²⁺ in NiO; satellite peak at 855.8 eV S(I) for Ni³⁺ in Ni₂O₃, Ni²⁺-OH species, and Ni²⁺ vacancies; and the other satellite peak at 861.3 eV S(II), involving a ligand-metal charge transfer (Salagre et al., 1996; Veenendaal and Sawatzky, 1993). The intensity ratio of S(I) to the main peak at 853.8 eV has been used to present the surface and/or structural density of defect sites (Solsona et al., 2012; Zhu et al., 2015), offering the information about the non-stoichiometric (or non-selective) property of NiO. Notably, this ratio declines from 4.0 for the NiO/Ni-foam-NS to 1.9 for the Nb₂O₅-NiO/Ni-foam-C, to 1.7 for the Nb₂O₅-NiO/Ni-foam-R, and further to 1.1 for the Nb₂O₅-NiO/Ni-foam-NS (Table S3). Clearly, Nb₂O₅ modification provides the ability to markedly reduce the non-stoichiometric Ni³⁺ (responsible for the non-selective O₂⁻ species), whereas the nanosheet NiO-precursor morphology synergistically promoted such Nb₂O₅ modification effect. This observation is in good agreement with the O₂-TPD results (Figure 3B). Figure 3D shows the XPS spectra in Nb3d region for the Nb₂O₅-NiO/Ni-foam catalysts. Taking the Nb⁵⁺ in pure Nb₂O₅ (207.4 eV) as reference (Liu et al., 2016), the BE of

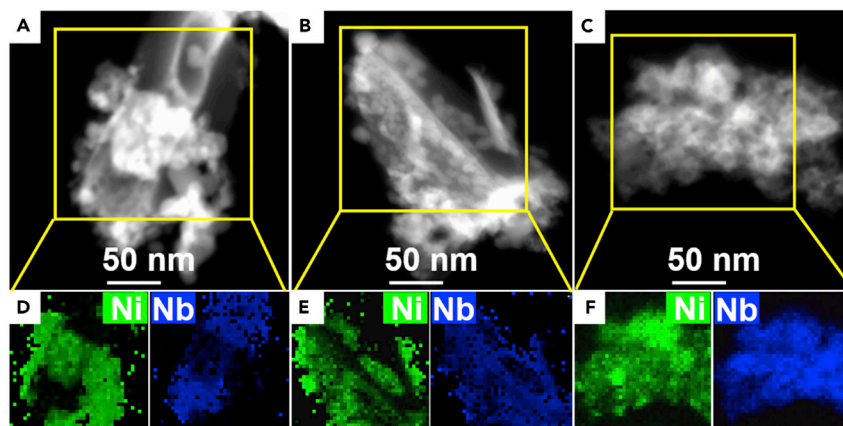


Figure 4. The Transmission Electron Microscopic Images of the Nb₂O₅-NiO/Ni-Foam Catalysts

(A–F) (A–C) High-angle annular dark-field scanning transmission electron microscopic images and (D–F) elemental maps of (A and D) Nb₂O₅-NiO/Ni-foam-C, (B and E) Nb₂O₅-NiO/Ni-foam-R, and (C and F) Nb₂O₅-NiO/Ni-foam-NS.

Nb⁵⁺ shifts to 207.2 eV for the Nb₂O₅-NiO/Ni-foam-C, 207.1 eV for the Nb₂O₅-NiO/Ni-foam-R, and then 206.9 eV for the Nb₂O₅-NiO/Ni-foam-NS. This trend is consistent with the increasingly stronger NiO-Nb₂O₅ interaction (Zhu et al., 2012).

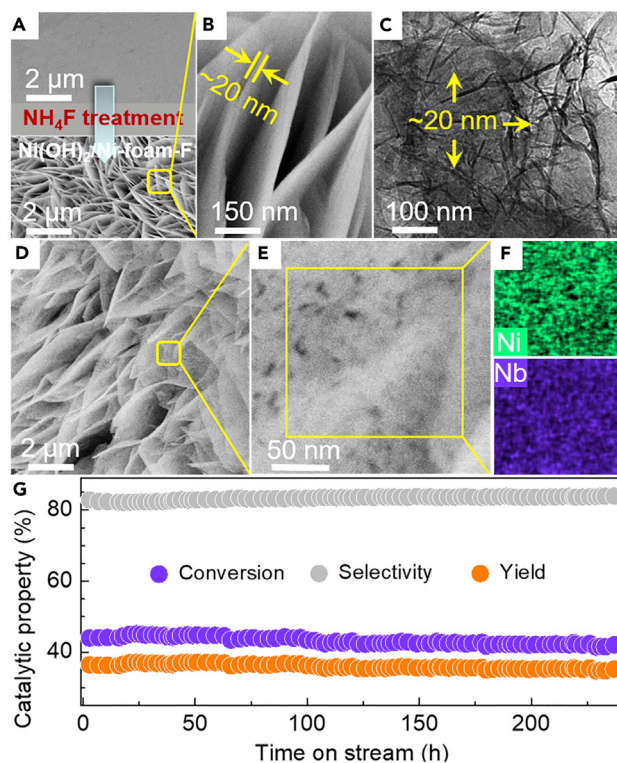


Figure 5. The Structure and Morphological Features of the Ni(OH)₂/Ni-foam-F Material and the Nb₂O₅-NiO/Ni-foam-F Catalyst and the Stability Test of the Nb₂O₅-NiO/Ni-foam-F Catalyst

(A–C) (A, upper) Scanning electron microscopic (SEM) image of the pristine Ni-foam. (A, lower, and B) SEM and (C) transmission electron microscopic images of Ni(OH)₂/Ni-foam-F.

(D–F) (D and E) SEM and (F) energy-dispersive X-ray images of Nb₂O₅-NiO/Ni-foam-F.

(G) Stability testing of Nb₂O₅-NiO/Ni-foam-F (reaction conditions: 400°C, C₂H₆/O₂/N₂ of 1/1/8, GHSV of 9,000 cm³ g⁻¹ h⁻¹).

Catalyst	C ₂ /O ₂ /Inert Molar Ratio	Temp. (°C)	GHSV (cm ³ g ⁻¹ h ⁻¹)	Conversion (%)	Selectivity (%)	TOF (h ⁻¹) ^a	Ref.
Nb ₂ O ₅ -NiO/Ni-foam-F	1/1/8	410	9,000	60	80	0.94	This work
NiNbO	1/1/8	400	6,600	65	71	0.37	Heracleous and Lemonidou (2006)
NiNbO/Al ₂ O ₃	1/1/9	400	6,600	27	70	0.84	Heracleous et al., 2005
NiTao	1/1/8	375	6,000	60	72	0.77	Zhu et al. (2015)
NiSnO	1/1/9	350	3,000	26	75	0.10	Solsona et al. (2012)
NiWO	2/2/17	400	6,000	52	60	–	Zhu et al., 2016
NiTio	2/2/17	400	6,000	50	66	–	Zhu et al., 2016
MoVNbTeO	3/2/5	400	2,120	59	89	–	Botella et al. (2004)
	9/6/85	400	780	87	84	–	

Table 2. Representative ODE Results for Reported NiO-Based and MoVTeNbO Catalysts

^aTOF is defined as the amount of ethylene formed per NiO site per hour.

As aforementioned, the nanosheet Ni-Tp precursor is much thinner than Ni(OH)₂ clump and NiC₂O₄ rod and is irregularly aligned to form a porous layer (Figures 1F, 1I, and 1L). This morphology undoubtedly gives higher SSA, which is helpful for highly dispersing Nb₂O₅ into the NiO matrix (Figures 1S, 1T, and 1U), leading to the lower Ni/Nb ratio in catalyst surface (Table S3); furthermore, as indicated by the high-angle annular dark-field scanning transmission electron microscopy images and elemental maps in Figures 4A–4F, the Nb₂O₅-NiO/Ni-foam-NS achieves the contacting of NiO with Nb₂O₅ more sufficient than the Nb₂O₅-NiO/Ni-foam-C and Nb₂O₅-NiO/Ni-foam-R. On the other hand, the thinner nanosheet feature of Ni-Tp facilitates the incorporation of Nb ions into NiO during calcination treatment. Indeed, the lattice constant obtained by XRD (Solsona et al., 2012) reveals that the NiO lattice constant in the Nb₂O₅-NiO/Ni-foam-NS is 4.1724 Å, smaller than 4.1767 Å for the NiO/Ni-foam and 4.1752 Å for both the Nb₂O₅-NiO/Ni-foam-C and Nb₂O₅-NiO/Ni-foam-R (Table 1). This observation evidences that Nb ions are, at least partially, incorporated into NiO to the most extent for the Nb₂O₅-NiO/Ni-foam-NS (Solsona et al., 2012; Zhu et al., 2012).

Design of the Advanced Catalyst

Last but not the least, according to the foregoing findings, we are confident that the ODE performance of Nb₂O₅-NiO/Ni-foam catalyst can be improved further if the NiO-precursor nanosheet is able to be thinned further. Indeed, the Ni(OH)₂ nanosheet (~20 nm) is successfully structured onto the Ni-foam by hydrothermal treatment in an aqueous solution of NH₄F (denoted as Ni(OH)₂/Ni-foam-F, Figures 5A–5C and S6), and therefore, a Nb₂O₅-NiO/Ni-foam-F catalyst was obtained by subsequent Nb₂O₅ modification. As expected, such catalyst shows much higher activity and selectivity than the Nb₂O₅-NiO/Ni-foam-C; when compared with the Nb₂O₅-NiO/Ni-foam-NS it achieves comparable activity but markedly improved selectivity (Figure S7). Notably, our Nb₂O₅-NiO/Ni-foam-F catalyst yields better performance (especially the selectivity, stability, and TOF) than the NiO-based catalysts (Tables 2 and S4) and powdered Nb₂O₅/NiO (5/21, w/w) catalyst literature (Table S5). Moreover, the ethylene yield (ethane conversion times ethylene selectivity) for such catalyst is comparable to the costly MoVTeNbO catalyst when it is tested at 2,120 cm³ g⁻¹ h⁻¹, but our catalyst runs at much higher reactor capacity (GHSV) of 9,000 cm³ g⁻¹ h⁻¹ (Table 2).

In addition, it is not surprising that the Nb₂O₅-NiO/Ni-foam-F exhibits highly enhanced Nb₂O₅-NiO interaction (Figures 5D–5F) by further thinning the NiO-precursor, which results in a further reduction of the NiO lattice constant (Table 1), the NiO nanoparticle size (Table 1 and Figure S6), and especially the non-selective O₂⁻ amount as well as the NiO reducibility (Figure S8), compared with the ones using Ni(OH)₂/Ni-foam-C (dense clump of Ni(OH)₂) and Ni-Tp/Ni-foam-NS (~30 nm Ni-Tp nanosheet). This is undoubtedly responsible for the further catalytic performance improvement observed on the Nb₂O₅-NiO/Ni-foam-F catalyst. Most notably, this catalyst exhibits favorable stability, being stable for at least 240 h at 400°C with ~44% ethane conversion and ~82% ethylene selectivity (Figure 5G), which shows great superiority when

compared with the previously reported Nb₂O₅-NiO catalysts (Table S4). This is benefited from the high Nb₂O₅-NiO sintering resistance (evidenced by the well-preserved SSA and particle size of NiO for the used catalyst, Table 1), as a result of the strong interaction between NiO and Nb₂O₅ (Solsona et al., 2011, 2012) in combination with the enhanced heat transfer of the Ni-foam-structured designing that could rapidly dissipate the large quantity of reaction heat from the ODE reaction (Table S5) (Li et al., 2015; Zhao et al., 2016; Zhang et al., 2018a, 2018b).

DISCUSSION

In summary, a low-temperature active, highly selective, and highly stable Nb₂O₅-NiO/Ni-foam catalyst has been developed for the ODE reaction, by carefully tuning the NiO-precursor morphology-dependent Nb₂O₅-NiO interaction. The Nb₂O₅-NiO interaction can be markedly improved by thinning the NiO-precursors endogenously grown onto the Ni-foam substrate, especially leading to significant elimination of the nonselective O₂⁻ species and, meanwhile, remarkable improvement of the mobility of selective O⁻ species. This work provides an interesting clue to tailor high-performance ODE catalyst via morphology modulation strategy.

Limitations of the Study

The ammonium niobium oxalate is a little bit costly.

METHODS

All methods can be found in the accompanying Transparent Methods supplemental file.

SUPPLEMENTAL INFORMATION

Supplemental Information can be found online at <https://doi.org/10.1016/j.isci.2019.09.021>.

ACKNOWLEDGMENTS

We acknowledge the financial supports from the Key Basic Research Project (grant 18JC1412100) from the Shanghai Municipal Science and Technology Commission, the National Natural Science Foundation of China (grants 21773069, 21703069, 21703137, 21473057, U1462129, 21273075), and the National Key Basic Research Program (grant 2011CB201403) from the Ministry of Science and Technology of the People's Republic of China.

AUTHOR CONTRIBUTIONS

Y. Lu, Z.Z., and G.Z. conceived the idea for the project and designed the experiments. Z.Z., G.Z., Y. Liu, and Y. Lu carried out the interpretation and wrote the manuscript. Z.Z. conducted the material synthesis, characterizations, and catalytic tests. W.S. drew the structure of Ni-foam in Figure 1. All authors discussed and commented on the manuscript. Y. Lu directed the research.

DECLARATION OF INTERESTS

Y. Lu, Z.Z., G.Z., and Y. Liu have a patent application related to this work filed with the Chinese Patent Office on October 15, 2017 (201710956118.5). The authors declare that they have no competing interests.

Received: May 3, 2019

Revised: August 6, 2019

Accepted: September 12, 2019

Published: October 25, 2019

REFERENCES

- Botella, P., García-González, E., Dejoz, A., López Nieto, J.M., Vázquez, M.I., and González-Calbet, J. (2004). Selective oxidative dehydrogenation of ethane on MoVTeNbO mixed metal oxide catalysts. *J. Catal.* 225, 428–438.
- Chen, P., Zhao, G.F., Shi, X.-R., Zhu, J., Ding, J., and Lu, Y. (2019). Nano-intermetallic InNi₃C_{0.5} compound discovered as a superior catalyst for CO₂ reutilization. *iScience* 17, 315–324.
- Fu, B., Lu, J., Stair, P.C., Xiao, G., Kung, M.C., and Kung, H.H. (2013). Oxidative dehydrogenation of ethane over alumina-supported Pd catalysts: effect of alumina overlayer. *J. Catal.* 297, 289–295.
- Gaab, S., Machli, M., Find, J., Grasselli, R., and Lercher, J. (2003). Oxidative dehydrogenation of ethane over novel Li/Dy/Mg mixed oxides: structure-activity study. *Top. Catal.* 23, 151–158.
- Heracleous, E., Lee, A.F., Wilson, K., and Lemonidou, A.A. (2005). Investigation of Ni-based alumina-supported catalysts for the

- oxidative dehydrogenation of ethane to ethylene: structural characterization and reactivity studies. *J. Catal.* **231**, 159–171.
- Heracleous, E., and Lemonidou, A.A. (2006). Ni-Nb-O mixed oxides as highly active and selective catalysts for ethene production via ethane oxidative dehydrogenation. Part I: characterization and catalytic performance. *J. Catal.* **237**, 162–174.
- Heracleous, E., and Lemonidou, A.A. (2010). Ni-Me-O mixed metal oxides for the effective oxidative dehydrogenation of ethane to ethylene—Effect of promoting metal Me. *J. Catal.* **270**, 67–75.
- Heynderickx, G., Schools, E., and Marin, G. (2005). Coke combustion and gasification kinetics in ethane steam crackers. *AIChE J.* **51**, 1415–1428.
- Iwamoto, M., Yoda, Y., Egashira, M., and Seiyama, T. (1976). Study of metal oxide catalysts by temperature programmed desorption. 1. Chemisorption of oxygen on nickel oxide. *J. Phys. Chem.* **80**, 1989–1994.
- Li, Y.K., Zhang, Q.F., Chai, R.J., Zhao, G.F., Liu, Y., and Lu, Y. (2015). CO₂ methanation: high-performance catalyst with enhanced heat transfer obtained by modified wet chemical etching of Ni-foam. *AIChE J.* **61**, 4323–4331.
- Liu, Y., Cong, P., Doolen, R.D., Guan, S., Markov, V., Woo, L., Zey, S., and Dingerdissen, U. (2003). Discovery from combinatorial heterogeneous catalysis: a new class of catalyst for ethane oxidative dehydrogenation at low temperatures. *Appl. Catal. A* **254**, 59–66.
- Liu, Y., Luo, L., Gao, Y., and Huang, W. (2016). CeO₂ morphology-dependent NbO_x-CeO₂ interaction, structure and catalytic performance of NbO_x/CeO₂ catalysts in oxidative dehydrogenation of propane. *Appl. Catal. B* **197**, 214–221.
- Mulla, S., Buyevskaya, O., and Baerns, M. (2001). Autothermal oxidative dehydrogenation of ethane to ethylene using Sr_xLa_{1.0}Nd_{1.0}O_y catalysts as ignitors. *J. Catal.* **197**, 43–48.
- Nakamura, K.I., Miyake, T., Konishi, T., and Suzuki, T. (2006). Oxidative dehydrogenation of ethane to ethylene over NiO loaded on high surface area MgO. *J. Mol. Catal. A* **260**, 144–151.
- Salagre, P., Fierro, J.L., Medina, F., and Sueiras, J.E. (1996). Characterization of nickel species on several γ -alumina supported nickel samples. *J. Mol. Catal. A* **106**, 125–134.
- Sattler, J., Ruiz-Martinez, J., Santillan-Jimenez, E., and Weckhuysen, B.M. (2014). Catalytic dehydrogenation of light alkanes on metals and metal oxides. *Chem. Rev.* **114**, 10613–10653.
- Savova, B., Loridant, S., Filkova, D., and Millet, J.M. (2010). Ni-Nb-O catalysts for ethane oxidative dehydrogenation. *Appl. Catal. A* **390**, 148–157.
- Skoufa, Z., Xantri, G., Heracleous, E., and Lemonidou, A.A. (2014). A study of Ni-Al-O mixed oxides as catalysts for the oxidative conversion of ethane to ethylene. *Appl. Catal. A* **471**, 107–117.
- Solsona, B., Concepción, P., Demicol, B., Hernández, S., Delgado, J.J., Calvino, J.J., and López Nieto, J.M. (2012). Selective oxidative dehydrogenation of ethane over SnO₂-promoted NiO catalysts. *J. Catal.* **295**, 104–114.
- Solsona, B., López Nieto, J.M., Concepción, P., Dejoz, A., Ivars, F., and Vázquezand, M.I. (2011). Oxidative dehydrogenation of ethane over Ni-W-O mixed metal oxide catalysts. *J. Catal.* **280**, 28–39.
- Veenendaal, M.A., and Sawatzky, G.A. (1993). Nonlocal screening effects in 2p x-ray photoemission spectroscopy core-level line shapes of transition metal compounds. *Phys. Rev. Lett.* **70**, 2459–2462.
- Wu, Y., Gao, J., He, Y.M., and Wu, T.H. (2012). Preparation and characterization of Ni-Zr-O nanoparticles and its catalytic behavior for ethane oxidative dehydrogenation. *Appl. Surf. Sci.* **258**, 4922–4928.
- Xu, H. (2017). Global ethylene industry in 2016 and its development trend. *Int. Petrol. Econ.* **3**, 101–106.
- Zhang, Z., Chai, R., Zhao, G., Liu, Y., and Lu, Y. (2018a). Oxidative dehydrogenation of ethane to ethylene: a promising CeO₂-ZrO₂-modified NiO-Al₂O₃/Ni-foam catalyst. *Appl. Catal. A* **550**, 151–159.
- Zhang, Z., Zhao, G., Chai, R., Zhu, J., Liu, Y., and Lu, Y. (2018b). Low-temperature, highly selective, highly stable Nb₂O₅-NiO/Ni-foam catalyst for the oxidative dehydrogenation of ethane. *Catal. Sci. Technol.* **8**, 4383–4389.
- Zhao, G.F., Liu, Y., and Lu, Y. (2016). Foam/fiber-structured catalysts: non-dip-coating fabrication strategy and applications in heterogeneous catalysis. *Sci. Bull.* **61**, 745–748.
- Zhu, B., Rosenfeld, D., Harb, M., and Anjum, D. (2016). Ni-M-O (M = Sn, Ti, W) catalysts prepared by a dry mixing method for oxidative dehydrogenation of ethane. *ACS Catal.* **6**, 2852–2866.
- Zhu, H., Rosenfeld, D., Anjum, D., Sangaru, S., Saih, Y., Ould-Chikh, S., and Basset, J. (2015). Ni-Ta-O mixed oxide catalysts for the low temperature oxidative dehydrogenation of ethane to ethylene. *J. Catal.* **329**, 291–306.
- Zhu, H.B., Ould-Chikh, S., Anjum, D.H., Sun, M., Biauxque, G., Basset, J.M., and Caps, V. (2012). Nb effect in the nickel oxide-catalyzed low-temperature oxidative dehydrogenation of ethane. *J. Catal.* **285**, 292–303.

ISCI, Volume 20

Supplemental Information

Oxidative Dehydrogenation of Ethane: Superior Nb₂O₅-NiO/Ni-Foam Catalyst Tailored by Tuning Morphology of NiO-Precursors Grown on a Ni-Foam

Zhiqiang Zhang, Guofeng Zhao, Weidong Sun, Ye Liu, and Yong Lu

Supplemental Information

Supplemental Tables

Table S1. Number of NiO sites for the Ni-foam structured catalysts, related to Table 1.

Catalyst	Number of NiO sites ($\times 10^{19} \text{ g}_{\text{cat}}^{-1}$) ^a
NiO/Ni-foam-C	7.2
NiO/Ni-foam-R	7.0
NiO/Ni-foam-NS	7.1
Nb ₂ O ₅ -NiO/Ni-foam-C	7.2
Nb ₂ O ₅ -NiO/Ni-foam-R	7.1
Nb ₂ O ₅ -NiO/Ni-foam-NS	10.1
Nb ₂ O ₅ -NiO/Ni-foam-F	10.6

^a Calculated by using the NiO density of 6.67 g cm^{-3} and the average crystallite diameter determined by XRD.

Table S2. The quantitative analysis of O₂-TPD results, related to Figure 3.

Catalyst	O ₂ ⁻ peak area	O ⁻ peak area	O ₂ ⁻ /O ⁻ ratio	Total area
NiO/Ni-foam-C	988	931	1.06	1920
NiO/Ni-foam-R	956	903	1.06	1859
NiO/Ni-foam-NS	964	917	1.05	1881
Nb ₂ O ₅ -NiO/Ni-foam-C	505	831	0.61	1336
Nb ₂ O ₅ -NiO/Ni-foam-R	457	792	0.56	1246
Nb ₂ O ₅ -NiO/Ni-foam-NS	167	552	0.30	719

Table S3. XPS results of the as-prepared catalysts, related to Figure 3.

Catalyst	Ni/Nb ratio in surface (at./at.)	Ni 2p _{3/2} (eV) ^a			Intensity ratio of S(I) to Main peak
		Main peak	BE satellite		
			I	II	
NiO/Ni-foam-NS	-	853.7	855.8	861.3	4.0
Nb ₂ O ₅ -NiO/Ni-foam-C	4.3	853.8	855.7	861.2	1.9
Nb ₂ O ₅ -NiO/Ni-foam-R	4.6	853.8	855.7	861.2	1.7
Nb ₂ O ₅ -NiO/Ni-foam-NS	6.7	853.9	855.7	861.2	1.1

^aEstimated experimental error of ± 0.1 eV.

Table S4. The results of stability test reported in the literature for the ODE reaction on the Nb₂O₅-NiO catalysts, related to Figure 5.

Catalyst	C ₂ /O ₂ /inert molar ratio	Temp. (°C)	GHSV (cm ³ g ⁻¹ h ⁻¹)	Time of stability test (h)	Conv. (%) ^a	Select. (%) ^a	Conv. (%)	Select. (%)	Loss of activity (%)	Ref.
Nb ₂ O ₅ -NiO/Ni-foam-F	1/1/8	400	6000	240	44	81	42	82	4.5	This work
NiNbO	2/1/17	330	6600	70	9	84	5	88	44.4	(Zhu et al., 2012)
NiNbO	1/1/9	380	6000	200	57	63	39	76	31.6	(Zhu et al., 2015)
NiNbO	2/2/17	330	6000	50	34	79	30	80	11.8	(Savova et al., 2010)

^aCatalytic performance after stability test of 1 h.

Table S5. Temperature-rising of the Ni-foam structured catalyst and powdered catalyst,^a related to Figure 5.

Catalyst	Temperature (°C)		C ₂ H ₆ Conv. (%)	Select. (%)	
	Furnace	Bed		C ₂ H ₄	CO ₂
Nb ₂ O ₅ /NiO (100-200 μm) (5/21, wt/wt)	340	353	16.8	84.4	16.6
	350	377	30.7	80.8	19.2
	360	395	42.5	77.6	22.4
	370	410	52.1	76.1	23.9
	380	422	56.6	74.7	25.1
Nb ₂ O ₅ -NiO/Ni-foam-F	350	352	15.7	88.6	11.4
	375	379	28.0	86.1	13.9
	400	408	44.0	82.7	17.3
	410	419	52.3	81.5	18.5
	425	436	59.8	80.0	20.0

^a Reaction conditions: C₂H₆/O₂/N₂ = 1/1/8, GHSV = 9000 cm³ g⁻¹ h⁻¹.

Supplemental figures

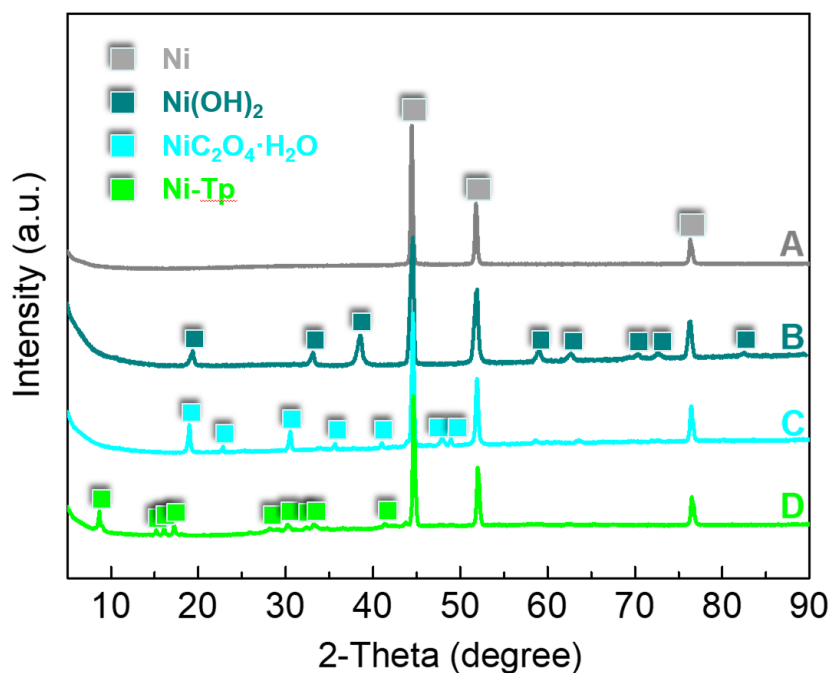


Figure S1. XRD patterns of the various NiO precursors, related to Figure 1. XRD patterns of (A) Ni-foam (showing metallic Ni diffraction peaks: 44.51°, 51.81°, 76.29°; JCPDS No. 04-0850), (B) Ni(OH)₂/Ni-foam (besides metallic Ni peaks, showing Ni(OH)₂ ones: 19.4°, 33.2°, 38.5°, 59.1°, 62.8°, 70.6°, 72.9° and 82.7°; JCPDS No. 14-0117), (C) NiC₂O₄·2H₂O/Ni-foam (besides metallic Ni peaks, showing NiC₂O₄·2H₂O ones: 18.9°, 22.7°, 30.5°, 35.4°, 40.9°, 47.7° and 48.9°; JCPDS No. 01-0299), and (D) Ni-Tp/Ni-foam (besides metallic Ni peaks, showing Ni-Tp ones: 8.7°, 15.2°, 16.2°, 17.3°, 28.1°, 30.3°, 32.4°, 33.3°, 41.4° and 43.4°; JCPDS No. 35-1677).

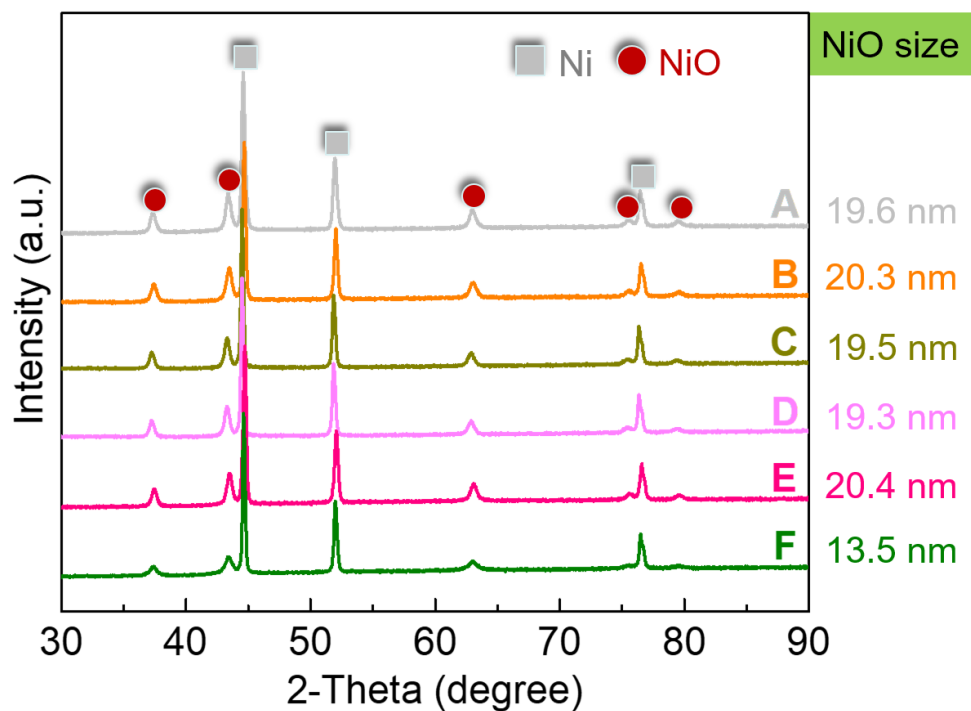


Figure S2. XRD patterns of the Ni-foam structured catalysts, related to Figure 1. XRD patterns of (A) NiO/Ni-foam-C, (B) NiO/Ni-foam-R, (C) NiO/Ni-foam-NS, (D) Nb₂O₅-NiO/Ni-foam-C, (E) Nb₂O₅-NiO/Ni-foam-R and (F) Nb₂O₅-NiO/Ni-foam-NS. *Note:* 21 wt% NiO; 5 wt% Nb₂O₅.

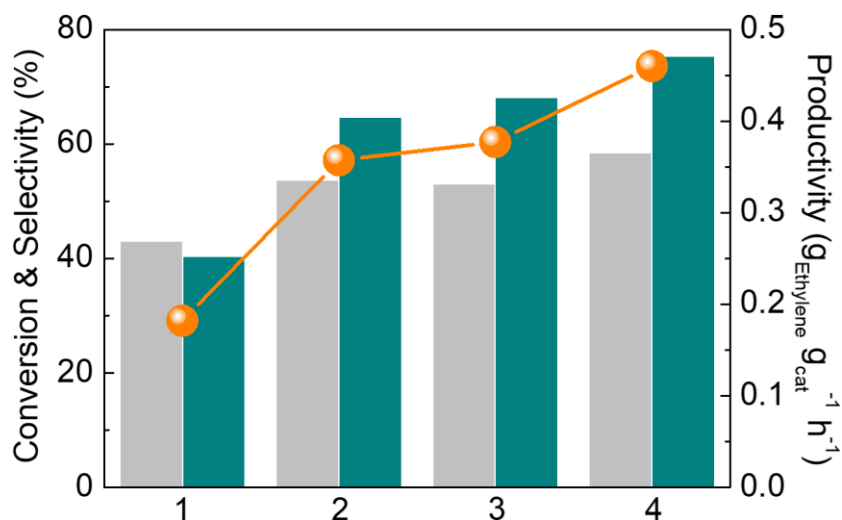


Figure S3. The ODE performance of the Ni-foam structured catalysts, related to Figure 2. Catalytic property of the as-prepared catalysts for ODE reaction. Note: ethane conversion (gray column), ethylene selectivity (cyan column) and productivity (orange line); 1: NiO/Ni-foam-NS; 2: Nb₂O₅-NiO/Ni-foam-C; 3: Nb₂O₅-NiO/Ni-foam-R; 4: Nb₂O₅-NiO/Ni-foam-NS. Reaction conditions: C₂H₆/O₂/N₂ of 1/1/8, 425 °C, GHSV of 9000 cm³ g⁻¹ h⁻¹.

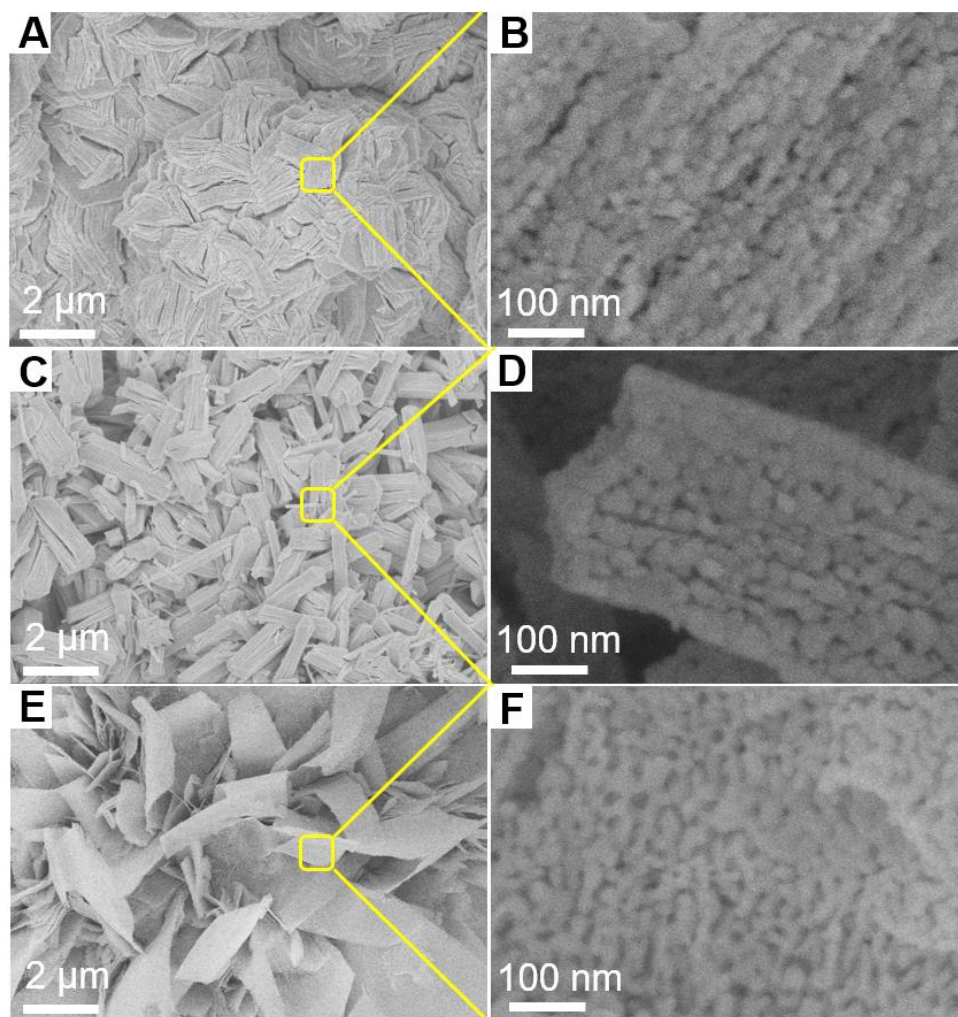


Figure S4. The structure and morphology features of the NiO/Ni-foam catalysts, related to Figure 2. SEM images of (A,B) NiO/Ni-foam-C, (C,D) NiO/Ni-foam-R and (E,F) NiO/Ni-foam-NS.

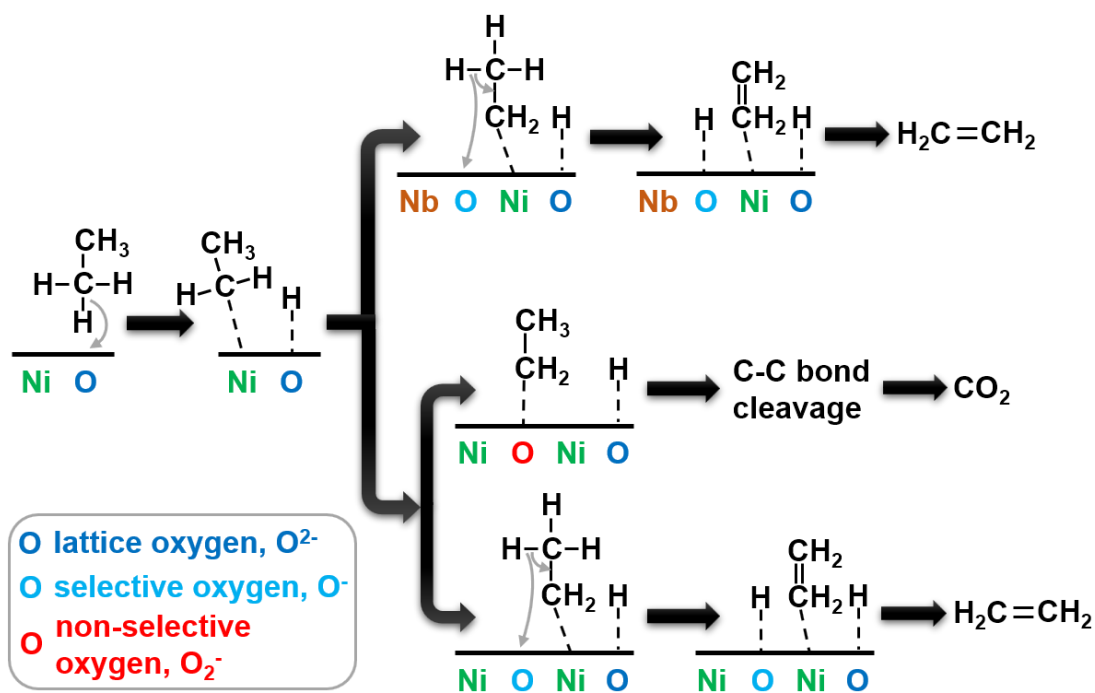


Figure S5. The schematic illustration of catalytic mechanism for ODE reaction over NiO/Ni-foam and Nb₂O₅-NiO/Ni-foam catalysts, related to Figure 2.

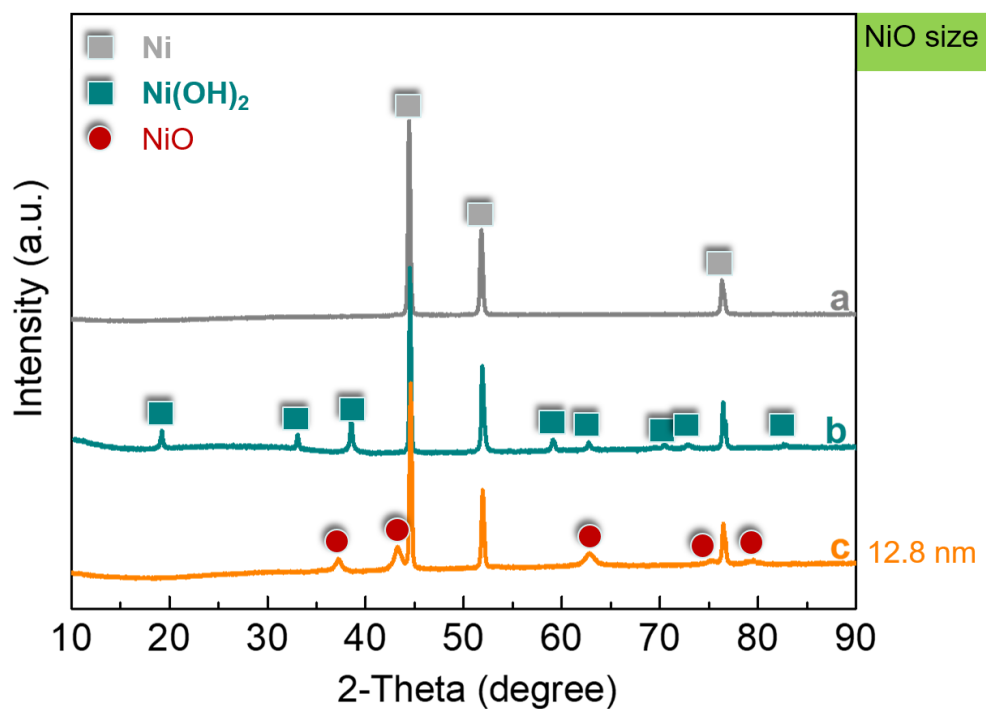


Figure S6. XRD patterns of the Ni-foam, Ni(OH)₂/Ni-foam-F, and Nb₂O₅-NiO/Ni-foam-F, related to Figure 5. XRD patterns of (A) Ni-foam, (B) Ni(OH)₂/Ni-foam-F, and (C) Nb₂O₅-NiO/Ni-foam-F.

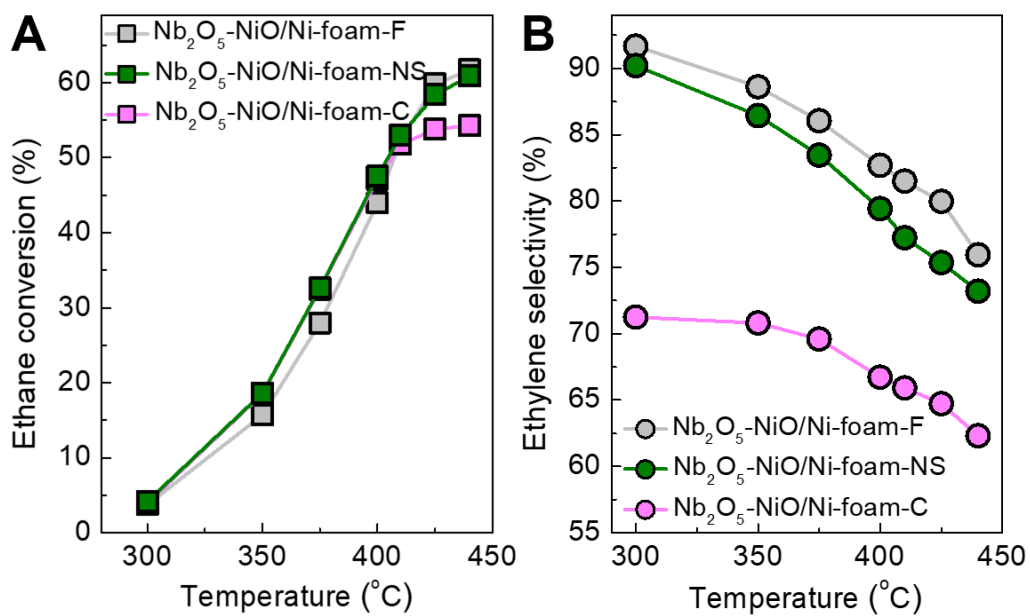


Figure S7. The ODE performance of the Ni-foam structured catalysts, related to Figure 5. Temperature-dependent (A) ethane conversion and (B) ethylene selectivity for the ODE reaction. Reaction conditions: C₂H₆/O₂/N₂ of 1/1/8, GHSV of 9000 cm³ g⁻¹ h⁻¹.

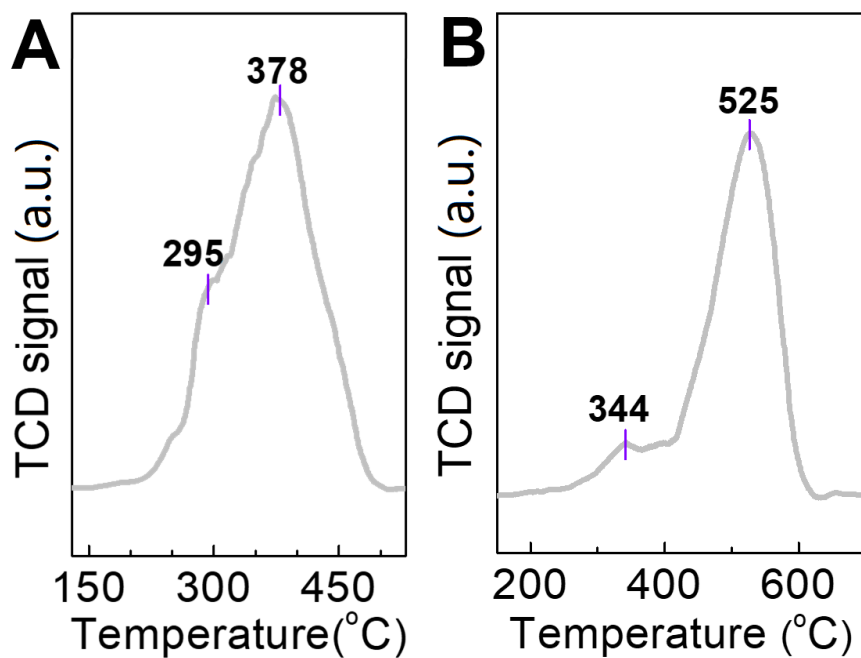


Figure S8. The characterization results of the Nb₂O₅-NiO/Ni-foam-F catalyst, related to **Figure 5**. (A) H₂-TPR and (B) O₂-TPD profiles for the Nb₂O₅-NiO/Ni-foam-F catalyst.

Transparent Methods

Preparation of catalysts

Pretreatment of pristine Ni-foam substrate. The pristine Ni-foam (purchased from Changsha Liyuan New Material Co. Ltd.) was carefully cleaned with 3 mol L⁻¹ HCl aqueous solution in an ultrasound bath for 10 min to remove the surface NiO layer, washed with deionized water and absolute ethanol for several times, and dried at 80 °C for 12 h.

Growth of clump-like Ni(OH)₂ onto Ni-foam. Ni(NO₃)₂·6H₂O of 10 mmol (2.91 g) and NH₄NO₃ of 6 mmol (0.48 g) were dissolved in deionized water of 48 mL. Then, NH₃·H₂O (28 wt%) of 6 mL was slowly added into the above solution drop by drop to obtain the nickel ammine solution. The mixed solutions were magnetically stirred for 20 min in air at room temperature. Afterwards, the as-cleaned Ni-foam (0.5 g) was immersed into the growth solution, and the in-situ growth of Ni(OH)₂ subsequently proceeded in water bath at 80 °C for 2 h. Finally, the resulted samples were rinsed with deionized water for several times and dried overnight at 80 °C to obtain the Ni(OH)₂/Ni-foam (Ye et al., 2016).

Growth of rod-like NiC₂O₄·2H₂O onto Ni-foam. Oxalic acid dihydrate of 15 mmol (1.89 g) and NH₄Cl of 1.5 mmol (0.081 g) were dissolved in deionized water of 50 mL. The solution was magnetically stirred for 20 min in air at room temperature and then transferred into a stainless steel Teflon-lined autoclave with 100 mL capacity. The as-cleaned Ni-foam (0.5 g) was immersed into the solution and then heated at 180 °C for 24 h. After the hydrothermal process, the resulted samples were rinsed with deionized water for several times and then dried overnight at 80 °C to obtain the NiC₂O₄/Ni-foam (Zhang et al., 2018).

Growth of nanosheet-like nickel terephthalate (Ni-Tp) onto Ni-foam. Terephthalic acid of 7 mmol (1.16 g) and Ni(NO₃)₂·6H₂O of 7 mmol (2.04 g) were dissolved in 50 mL of N,N-dimethylformamide (DMF). The solution was magnetically stirred for 20 min in air at room temperature and then transferred into a stainless steel Teflon-lined autoclave with 100 mL capacity. The as-cleaned Ni-foam (0.5 g) was immersed into the solution and heated at 150 °C for 24 h. After the hydrothermal process, the resulted samples were rinsed successively with deionized water and absolute ethanol for several times and then dried overnight at 80 °C to obtain the Ni-Tp/Ni-foam (Chen et al., 2017).

Growth of nanosheet-like Ni(OH)₂ onto Ni-foam. Ni(NO₃)₂·6H₂O of 4 mmol (2.33 g) and CO(NH₂)₂ of 20 mmol (2.40 g) were dissolved in 30 mL aqueous solution of NH₄F (containing NH₄F of 8 mmol, 0.592 g). The solution was magnetically stirred for 20 min in air at room temperature and then transferred into a stainless steel Teflon-lined autoclave with 100 mL capacity. The as-cleaned Ni-foam (0.5 g) was immersed into the solution and heated at 100 °C for 12 h. After the hydrothermal process, the resulted samples were rinsed successively with deionized water several times and then dried overnight at 80 °C to obtain the Ni(OH)₂/Ni-foam-F (Huang et al., 2014).

Preparation of NiO/Ni-foam catalysts. The as-obtained Ni(OH)₂/Ni-foam, NiC₂O₄/Ni-foam, Ni-Tp/Ni-foam, and Ni(OH)₂/Ni-foam-F samples were calcined in air at 450 °C for 2 h to form the NiO/Ni-foam-C, NiO/Ni-foam-R, NiO/Ni-foam-NS, and NiO/Ni-foam-F catalysts, respectively.

Preparation of Nb₂O₅-NiO/Ni-foam catalysts. The as-obtained Ni(OH)₂/Ni-foam, NiC₂O₄/Ni-foam, Ni-Tp/Ni-foam, and Ni(OH)₂/Ni-foam-F samples were directly impregnated

with an aqueous solution of ammonium niobium oxalate of specific concentration in the incipient wetness manner. After drying at 100 °C overnight and calcining in air at 450 °C for 2 h, the Nb₂O₅-NiO/Ni-foam-C, Nb₂O₅-NiO/Ni-foam-R, Nb₂O₅-NiO/Ni-foam-NS, and Nb₂O₅-NiO/Ni-foam-F catalysts were obtained, respectively. Note that the loadings of NiO and Nb₂O₅ could be tuned via controlling the preparation conditions of different NiO precursors and added amount of ammonium niobium oxalate, respectively.

Preparation of the powdered Nb₂O₅-NiO catalyst. The nanosheet-like Ni(OH)₂ powders were obtained by solvothermal method using the solution of Ni(NO₃)₂, CO(NH₂)₂ and NH₄F in 100 °C for 12 h (Huang et al., 2014). The powdered catalyst Nb₂O₅/NiO (5/21, wt/wt; 100-200 μm) was prepared by impregnation of nanosheet-like Ni(OH)₂ powders with niobium ammonium oxalate solution followed by calcination in air at 450 °C.

Characterization of catalysts

Crystalline phases of all catalysts were probed by X-ray diffraction (XRD, Rigaku Ultima IV) in the 2θ scanning range of 20-90° at a scanning rate of 10°/min, using the Cu Kα radiation source generated at 30 kV and 25 mA. Particle size of NiO was calculated by the Scherrer equation at 2θ of 43.3°. N₂ adsorption/desorption isotherms were measured at 77 K on a BEL-MAX gas adsorption analyzer. Prior to the measurement, the samples were degassed for 6 h at 100 °C before nitrogen adsorption. Specific surface area (SSA) was calculated from the adsorption branch in the range of relative pressure from 0.05 to 0.25 by Brunauer-Emmett-Teller (BET) method. Catalyst geometry and morphology were characterized by scanning electron microscopy (SEM, Hitachi S-4800, Japan) with an energy dispersive X-ray spectrometry (EDX) and transmission electron microscopy (TEM, FEI-Tecnaï G2F30). Reducibility of NiO species for the catalysts was analyzed by H₂-temperature programmed reduction (H₂-TPR) while the NiO content was calculated on the basis of H₂ consumption data deduced from H₂-TPR experiments (Li et al., 2015). Distribution and amount of surface oxygen species for the catalysts was analyzed by O₂-temperature programmed desorption (O₂-TPD). H₂-TPR and O₂-TPD experiments were all performed on a TP 5080 multi-functional automatic adsorption instrument (Xianquan Industrial and Trading Co., Ltd) with a thermal conductivity detector (TCD). For each H₂-TPR trial, sample (100 mg) purged by He at 450 °C for 30 min in advance was heated from 25 to 600 °C in a gas mixture of 10% H₂ in N₂ (30 mL min⁻¹) at a heating ramp of 10 °C min⁻¹. For each O₂-TPD trial, sample (200 mg) was treated at 450 °C for 30 min and cooled down to room temperature (r.t.) in a 3 vol % O₂/He flow (30 mL min⁻¹). After that, the sample flushed in He carrier flow (30 mL min⁻¹) until a horizontal TCD baseline appeared was heated from r.t. to 850 °C at a heating rate of 15 °C min⁻¹. The non-stoichiometric property of the catalysts was analyzed by X-ray photoelectron spectroscopy (XPS), which was recorded on an Escalab 250xi spectrometer, using a standard Al Kα X-ray source (300 W) and an analyzer pass energy of 20 eV. All binding energies were referenced to the adventitious C1s line at 284.6 eV.

ODE Reaction Test

The ODE reaction with molecular oxygen was performed in a fixed-bed quartz tube reactor

(i.d., 8 mm; reactor length of 700 mm) under atmospheric pressure using a gas hourly space velocity (GHSV) of $9,000 \text{ cm}^3 \text{ g}^{-1} \text{ h}^{-1}$. Circular chips (8.1 mm diameter) of the catalysts were packed layer-by-layer into the tube reactor with and the catalyst dosage was 0.2 g. Note that the diameter of 0.1 mm larger than the i.d. of the tubular reactor was retained deliberately to avoid the appearance of gap between the reactor wall and the edges of catalyst chips thereby preventing the gas bypassing. In addition, the powdered $\text{Nb}_2\text{O}_5/\text{NiO}$ catalyst of 52 mg (i.e., equivalent amount of Nb_2O_5 plus NiO to that for the $\text{Nb}_2\text{O}_5\text{-NiO/Ni-foam-F}$ catalyst) was dosed into reactor, and was diluted using quartz sand to obtain the equivalent bed volume to that for the $\text{Nb}_2\text{O}_5\text{-NiO/Ni-foam-F}$ catalyst. The catalyst bed was then heated from r.t. to the reaction temperature ranged from 300 to 450 °C in a gaseous $\text{C}_2\text{H}_6/\text{O}_2/\text{N}_2$ mixture (molar ratio of 1/1/8). Three calibrated mass flow controllers were used to control the oxygen, nitrogen and ethane gas, of which the purity is $> 99.99\%$. Effluent gas was analyzed by an online HP 6850 gas chromatograph equipped with a thermal conductivity detector (TCD) connected to Plot U and MS 5A parallel capillary columns (DIKMA). A Plot U column was used to separate CO_2 , C_2H_4 , and C_2H_6 and a 5A molecular sieve column was used to separate O_2 , N_2 , CH_4 , and CO . Notably, CO_2 was the only byproduct detected and no CO was observed owing to the CO oxidation to CO_2 (Han et al., 2014) under our conditions. No coke was found on the catalyst during the ODE reaction test. Moreover, the mass balance calculated on the basis of carbon lies in 98-100%.

TOF Calculation

In order to further assess the intrinsic catalytic activity, so called turnover frequency (TOF) which is defined as the amount of ethylene formed per NiO site per hour (Solsona et al., 2012) are calculated and C_2H_6 conversion was controlled to be $< 5\%$ at 300 °C. The theoretical specific surface area (SSA) of catalyst is expressed as S , the area of one NiO-unity is expressed as $S(\text{NiO})$ and the theoretical total surface area of catalyst is expressed as S_{Total} . The a is the NiO loading and the NiO density ($\rho(\text{NiO})$) is 6.67 g cm^{-3} (Zhu et al., 2015). In addition, b is the half of NiO lattice constant and $F(\text{C}_2\text{H}_6)$ is the flow of C_2H_6 (L/h). Accordingly, the theoretical number of NiO sites ($N(\text{NiO})$) and TOF can be expressed as follows, assuming that the NiO hemispheres are exposed on catalyst surface.

$$S = \frac{S_{\text{Total}}}{m(\text{Cat})} = \frac{\frac{a * m(\text{Cat})}{\rho(\text{NiO})} * \frac{1}{2} * 4 * \pi * r(\text{NiO})^2}{\frac{1}{2} * \frac{4}{3} * \pi * r(\text{NiO})^3 * m(\text{Cat})} = \frac{3 * a}{r(\text{NiO}) * \rho(\text{NiO})}$$

$$N(\text{NiO}) = \frac{S}{S(\text{NiO})} = \frac{3 * a}{\pi * b^2 * r(\text{NiO}) * \rho(\text{NiO})} = \frac{3 * a}{\pi * b^2 * r(\text{NiO}) * \rho(\text{NiO})}$$

$$TOF = \frac{Yield(\text{C}_2\text{H}_4) * N(\text{C}_2\text{H}_6)}{N(\text{NiO})} = \frac{Conv(\text{C}_2\text{H}_6) * Sel(\text{C}_2\text{H}_4) * n(\text{C}_2\text{H}_6) * N_A}{\frac{3 * a}{\pi * b^2 * r(\text{NiO}) * \rho(\text{NiO})}}$$

$$= \frac{Conv(\text{C}_2\text{H}_6) * Sel(\text{C}_2\text{H}_4) * P * F(\text{C}_2\text{H}_6) * N_A * \pi * b^2 * r(\text{NiO}) * \rho(\text{NiO})}{3 * a * R * T}$$

Supplementary References

Chen, Q., Lei, S., Deng, P., Ou, X., Chen, L., Wang, W., Xiao, Y., and Cheng, B. (2017). Direct growth of nickel terephthalate on Ni foam with large mass-loading for high-performance supercapacitors. *J. Mater. Chem. A* 5, 19323-19332.

Chu, B., An, H., Nijhuis, T.A., Schouten C., and Cheng, Y. (2015). A self-redox pure-phase M1 MoVNbTeO_x/CeO₂ nanocomposite as a highly active catalyst for oxidative dehydrogenation of ethane. *J. Catal.* 329, 471-478.

Han, S.W., Kim, D.H., Jeong, M.G., Park, K.J., and Kim, Y.D. (2016). CO oxidation catalyzed by NiO supported on mesoporous Al₂O₃ at room temperature. *Chem. Eng. J.* 283, 992-998.

Heracleous, E., and Lemonidou, A.A. (2006). Ni-Nb-O mixed oxides as highly active and selective catalysts for ethene production via ethane oxidative dehydrogenation. Part I: Characterization and catalytic performance. *J. Catal.* 237, 162-174.

Heracleous, E., Lee, A.F., Wilson, K., and Lemonidou, A.A. (2005). Investigation of Ni-based alumina-supported catalysts for the oxidative dehydrogenation of ethane to ethylene: structural characterization and reactivity studies. *J. Catal.* 231, 159-171.

Huang, M., Li, F., Ji, J., Zhang, Y., Zhao, X., and Gao, X. (2014). Facile synthesis of single-crystalline NiO nanosheet arrays on Ni foam for high-performance supercapacitors. *CrystEngComm* 16, 2878-2884.

Li, Y.K., Zhang, Q.F., Chai, R.J., Zhao, G.F., Liu, Y., and Lu, Y. (2015). Structured Ni-CeO₂-Al₂O₃/Ni-foam catalyst with enhanced heat transfer for substitute natural gas production by syngas methanation. *ChemCatChem* 7, 1427-1431.

Savova, B., Loridant, S., Filkova, D., and Millet, J.M. (2010). Ni-Nb-O catalysts for ethane oxidative dehydrogenation. *Appl. Catal. A* 390, 148-157.

Solsona, B., Concepción, P., Demicol, B., Hernández, S., Delgado, J.J., Calvino, J.J., and López Nieto, J.M. (2012). Selective oxidative dehydrogenation of ethane over SnO₂-promoted NiO catalysts. *J. Catal.* 295, 104-114.

Ye, K., Zhang, H., Zhao, L., Huang, X., Cheng, K., Wang, G., and Cao, D. (2016). Facile preparation of three-dimensional Ni(OH)₂/Ni foam anode with low cost and its application in a direct urea fuel cell. *New J. Chem.* 40, 8673-8680.

Zhang, Z., Zhao, G., Chai, R., Zhu, J., Liu, Y., and Lu, Y. (2018). Low-temperature, highly selective, highly stable Nb₂O₅-NiO/Ni-foam catalyst for the oxidative dehydrogenation of ethane. *Catal. Sci. Technol.* 8, 4383-4389.

Zhu, H., Dong, H., Laveille, P., Saih, Y., Caps, V., and Basset, J. (2014). Metal oxides modified NiO catalysts for oxidative dehydrogenation of ethane to ethylene. *Catal. Today* 228, 58-64.

Zhu, H., Rosenfeld, D., Anjum, D., Sangaru, S., Saih, Y., Ould-Chikh, S., and Basset, J. (2015). Ni-Ta-O mixed oxide catalysts for the low temperature oxidative dehydrogenation of ethane to ethylene. *J. Catal.* 329, 291-306.

Zhu, H.B., Ould-Chikh, S., Anjum, D.H., Sun, M., Biauxque, G., Basset, J.M., and Caps, V. (2012). Nb effect in the nickel oxide-catalyzed low-temperature oxidative dehydrogenation of ethane. *J. Catal.* 285, 292-303.

Zhu, H.B., Rosenfeld, D.C., Anjum, D.H., Caps, V., and Basset, J.M. (2015). Green synthesis of Ni-Nb oxide catalysts for low-temperature oxidative dehydrogenation of ethane. *ChemSusChem* 8, 1254-1263.